International Journal of Robotics and Control Systems
Vol. 5, No. 5, 2025, pp. 2399-2413
ISSN 2775-2658
http://pubs2.ascee.org/index.php/ijrcs

Frequency-Domain Modeling and PI-Lead Controller Design for Non-Ideal DC-DC Boost Converters

Duc Minh Ngo [a,1], Dzung Tien Nguyen [a,2,*], Thao Thanh Thi Tran [a,3]

[a] Thai Nguyen University of Technology, Thai Nguyen 250000, Vietnam
[1] ngoduc198-tdh@tnut.edu.vn; [2] dungnguyentien@tnut.edu.vn; [3] tranthanhthaoktd@tnut.edu.vn
* Corresponding Author

ARTICLE INFO

Article history
Received August 16, 2025
Revised September 24, 2025
Accepted November 17, 2025

Keywords
DC-DC Boost Converter;
State-Space Averaging Technique;
PI-Lead Controller;
Frequency-Domain Design;
Non-Ideal Modeling

ABSTRACT

In most previous studies, DC-DC converters were modeled under ideal assumptions. This study develops a more realistic mathematical model by explicitly incorporating non-ideal effects such as parasitic resistances of inductors, capacitors, MOSFETs, and diodes, as well as the diode forward voltage drop. A conventional PI controller tuned via the Stability Boundary Locus method has been applied in prior work, but it often suffers from limited gain crossover frequency and prolonged settling time, leading to degraded transient performance. To overcome these limitations, a PI-lead controller design is proposed, in which controller parameters are systematically tuned based on desired phase margin and gain crossover frequency. The PI part enhances low-frequency gain and ensures steady-state accuracy, while the lead part contributes additional phase margin, thereby improving dynamic response. Simulation results indicate that the proposed PI-lead strategy provides faster settling response, reduced overshoot, and improved stability compared to the traditional PI controller. These improvements, summarized through both frequency- and time-domain analyses, demonstrate the potential of PI-lead control for real-world applications such as renewable energy systems, electric vehicles, and aerospace power electronics. The main contribution of this work is the integration of comprehensive non-ideal modeling with frequency-domain-based PI-lead tuning, providing both theoretical insights and practical significance. These results highlight the potential of PI-lead control for high-performance applications such as renewable energy systems, electric vehicles, and aerospace power electronics.

1. Introduction

DC-DC boost converters have become indispensable in modern power electronics due to their capability to efficiently step up a low and unstable DC voltage into a higher, regulated output. They are widely employed in renewable energy systems (e.g., photovoltaic and fuel-cell power generation), automotive electronics, aerospace systems, and portable devices, where maintaining a stable DC bus voltage is critical for reliable operation [1]-[12]. Despite their widespread application, designing a boost converter that operates robustly under varying load and input conditions remains a significant challenge. The unregulated nature of typical input sources, such as solar panels or batteries, combined

with fluctuating loads, demands advanced modeling and control strategies to guarantee both high efficiency and stable performance [13]-[19].

Traditionally, most converter models and controller designs have assumed ideal conditions, neglecting the parasitic effects of inductors, capacitors, MOSFETs, and diodes. While such simplifications are useful for preliminary analysis, they fail to capture the real dynamics of converters operating at high frequencies or under significant load variations [20]-[28]. In practice, parasitic resistances, MOSFET on-state resistance, diode forward voltage drops, and equivalent series resistance (ESR) of capacitors significantly impact efficiency, voltage gain, and dynamic behavior [29]-[36]. Therefore, incorporating non-idealities into the mathematical model is essential for accurate performance prediction and for designing controllers that can handle real-world operating conditions. Recent studies have shown that ignoring these effects can lead to inaccurate small-signal models, degraded transient response, and even instability under certain operating scenarios [37]-[42].

Control of boost converters has been an active research topic for decades. Conventional linear controllers such as PI and PID remain popular due to their simplicity and ease of implementation. In the frequency domain, the proportional-integral (PI) controller improves low-frequency gain and eliminates steady-state error, making it attractive for output voltage regulation [43]-[46]. However, PI controllers typically limit the gain crossover frequency, resulting in slower transient responses and prolonged settling times [47]-[50]. Moreover, in non-ideal boost converters where additional poles and zeros emerge due to parasitic components, conventional PI controllers may fail to provide adequate phase margin, leading to overshoot and degraded stability [51]-[54].

To overcome these limitations, researchers have explored advanced control strategies such as adaptive PI tuning, model predictive control (MPC), sliding-mode control (SMC), passivity-based control, and other nonlinear methods [55]-[58]. Although these advanced techniques offer enhanced robustness, they are often computationally intensive and require more complex implementation, which may limit their practicality in low-cost embedded systems. A more feasible alternative is to augment the conventional PI controller with a lead compensator, resulting in a PI-lead controller. The PI-lead structure combines the strengths of both components: the PI term boosts low-frequency gain and ensures steady-state accuracy, while the lead term provides additional phase margin around the gain crossover frequency, thereby improving transient response and reducing overshoot [59]-[60].

Unlike prior studies, this work explicitly positions the PI-lead controller, tuned in the frequency domain, as a novel and practical integration for applications requiring stable and reliable power delivery, such as electric vehicles, drones, and robotics. In frequency-domain analysis, key performance metrics such as phase margin and gain crossover frequency play a decisive role in balancing stability and dynamic speed. A higher phase margin generally implies better robustness and lower overshoot, while a higher gain crossover frequency improves response speed at the cost of increased noise sensitivity. Careful tuning of the PI-lead controller using these criteria makes it possible to achieve both fast transient response and accurate steady-state regulation in non-ideal boost converters [61]. The research gap identified here is that conventional PI controllers cannot adequately achieve this trade-off in non-ideal boost converters, and advanced methods, while effective, are often impractical for embedded implementation. This motivates the PI-lead solution as both theoretically sound and practically feasible

This work addresses these challenges by integrating non-ideal modeling with a frequency-domain PI-lead design approach. The contributions of this work can be summarized as follows: (1) Comprehensive non-ideal modeling of the DC-DC boost converter, including inductor resistance, capacitor ESR, diode forward voltage, and MOSFET losses. (2) PI-lead controller design guided by frequency-domain criteria, ensuring improved dynamic response and stability. (3) Analytical tuning algorithm to compute controller parameters based on desired phase margin and gain crossover frequency. (4) Performance validation via simulation, demonstrating faster settling times, reduced overshoot, and higher robustness compared to conventional PI controllers.

The remainder of this paper is structured as follows: Section 2 develops the mathematical model of the non-ideal DC-DC boost converter. Section 3 presents the design of the PI-lead controller using

frequency-domain analysis and compares results with a traditional PI controller. Section 4 concludes with key findings and directions for future research.

2. Modeling of Non-Ideal DC-DC Boost Converter

The circuit diagram of the non-ideal DC-DC boost converter is illustrated in Fig. 1. The first step in the mathematical modeling of power DC-DC converters is to derive a linearized model. In DC-DC converters, the inductor currents and capacitor voltages are typically chosen as state variables, with their total number corresponding to the number of inductors and capacitors in the system. Since the DC-DC boost converter is a second-order system, its mathematical model consists of two state variables. To develop a comprehensive mathematical representation of the non-ideal DC-DC boost converter, the state-space averaging technique is employed. The key steps involved in this modeling process are outlined below, with a more detailed procedure provided in [11].

In the state-space averaging approach, the system dynamics are first expressed for each switching interval (ON and OFF states), including the effects of parasitic resistances and diode forward voltage. The time-averaged state equations are then obtained by weighting each subinterval equation according to the duty ratio D. This procedure results in a continuous-time averaged model that captures the influence of parasitic elements while smoothing out the switching behavior. The use of averaging under non-ideal conditions is justified by prior studies [2], [11], which show that parasitic resistances can be incorporated linearly without invalidating the averaging framework, provided that switching frequency is sufficiently higher than the system bandwidth.

- **Step 1**: Obtaining the state equation for each circuit state

According to Fig. 2 when the switch is on, the following equations are obtained by using KVL and KCL formula.

$$v_L(t) = V_g(t) - i_L(t)(r_L + r_{sw}) \tag{1}$$

$$i_C(t) = -\frac{v_C(t)}{R + r_C} \tag{2}$$

$$v_o(t) = v_C(t) + i_C(t)r_C \tag{3}$$

From Fig. 3 when the switch is off, we get

$$v_L(t) = L\frac{di_L(t)}{dt} = V_g(t) - V_d - (r_{sw} + R_L)i_L(t) - v_o(t) \tag{4}$$

$$i_C(t) = C\frac{dv_C(t)}{dt} = i_L(t) - \frac{v_o(t)}{R} \tag{5}$$

$$v_o(t) = v_C(t) + r_C i_C(t) \tag{6}$$

- **Step 2**: Finding the averaged state-space model
- **Step 3**: Linearization by introducing small ac perturbation around a DC operating point
- **Step 4**: Determination of various transfer function from small-signal model

From the averaged state equations, small-signal perturbation and linearization are applied around the operating point to derive the control-to-output transfer function. Each step in this transition—from time-domain averaged dynamics to the small-signal model—is detailed to ensure reproducibility. It is important to note that parasitic elements introduce additional poles and zeros, which are explicitly retained in the derived transfer function. This provides a more accurate representation of non-ideal converter dynamics compared to models that neglect parasitics.

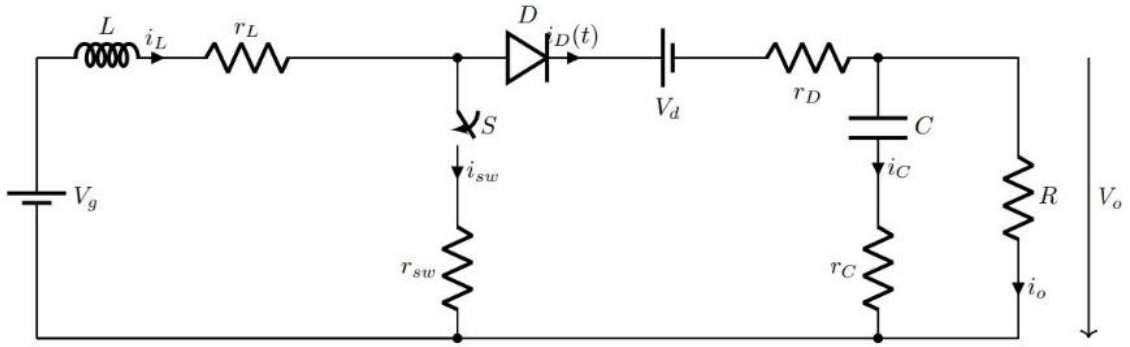

Fig. 1. Circuit diagram of non-ideal DC-DC boost converter

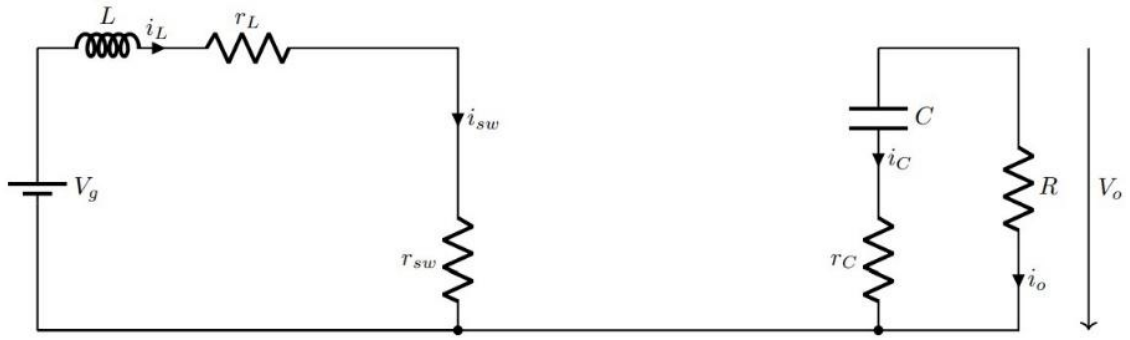

Fig. 2. Equivalent circuit during switch on

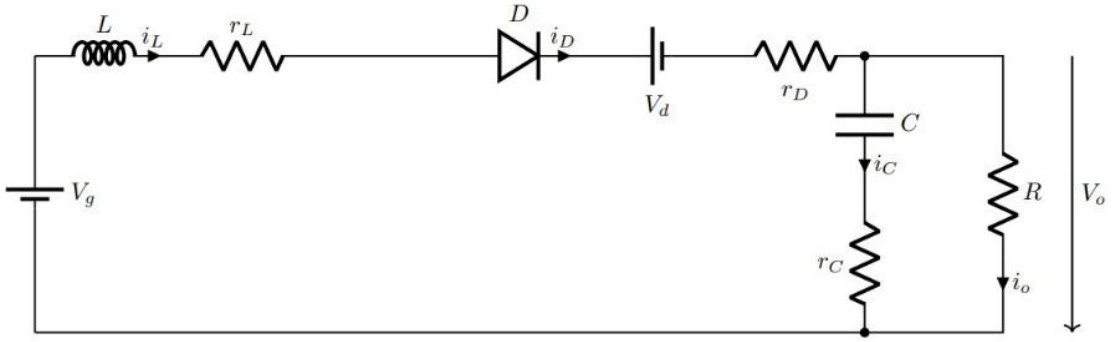

Fig. 3. Equivalent circuit during switch off

From [2] with detail converter specifications shown in Table 1, the duty cycle to output voltage transfer function is given.

$$G_{vd}(s) = \frac{-0.4227s^2 - 1.2812 \times 10^5 s + 9.4057 \times 10^{10}}{s^2 + 4.1760 \times 10^4 s + 3.2433 \times 10^9} \quad (7)$$

The above expression is fundamentally used to analyze the non-ideal DC-DC boost converter.

Table 1. Non-ideal DC-DC boost converter specifications

Parameters	Value	Parameters	Value
Input voltage, V_g	5 V	Diode forward voltage, V_d	0.555 V
Output voltage, V_o	12 V	Resistance switch/diode (r_{sw}/r_d)	0.024 Ω / 0.031 Ω
Load resistance, R	12 Ω	Switching frequency, f	500 kHz
Capacitance, C/r_C	4.7 µH / 0.071 Ω	Duty ratio, D	0.6285

The Bode plots of both the ideal and non-ideal DC-DC boost converters are presented in Fig. 4. The phase margins for the ideal and non-ideal cases are -75° (at 52 kHz) and -12° (at 67 kHz),

respectively. These results indicate that the closed-loop system of the non-ideal DC-DC boost converter exhibits greater stability compared to its ideal counterpart. Additionally, the step responses of the ideal and non-ideal DC-DC boost converters are illustrated in Fig. 5. The non-ideal case demonstrates reduced overshoot and oscillations, which can be attributed to the damping effect introduced by parasitic resistances.

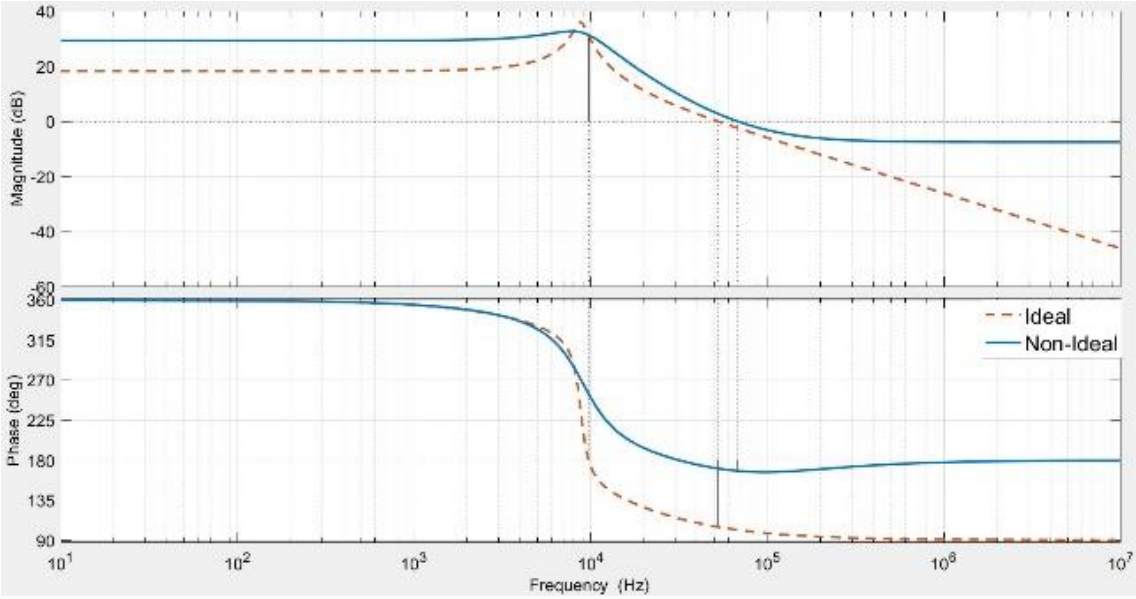

Fig. 4. Comparison of Bode plots of G_{vd} (s) for ideal and non-ideal boost converter

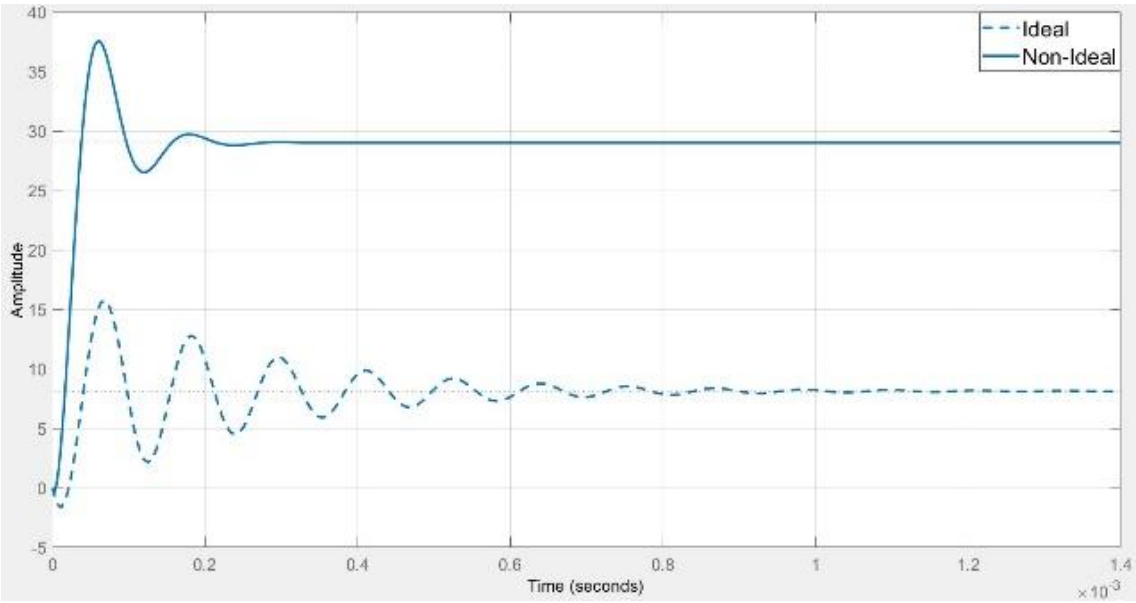

Fig. 5. Comparison of step responses of $G_{vd}(s)$ for ideal and non-ideal boost converter

It should be noted that a negative phase margin corresponds to instability. In our revised interpretation, the results indicate that the non-ideal model introduces additional phase lag, which can reduce stability margins if not properly compensated. The proposed PI-lead controller directly addresses this issue by improving the phase margin and ensuring stable operation

3. PI-Lead Controller Design Based on Frequency Domain Measures

For an effective control system, the frequency response must meet the following criteria: (i) ideally, the Bode plot should exhibit a slope of -20 dB/decade in the low-frequency region; (ii) the

phase margin of the compensated system should be greater than 60° to ensure robust closed-loop stability against disturbances; and (iii) the gain crossover frequency of the compensated system should fall within the range of one-tenth to one-fourth of the converter's switching frequency [4], [11]. To achieve high-performance control of the converter, an accurate mathematical model is essential.

- **PI controller**: The transfer function of PI controller is obtained as

$$G_{pi}(s) = \frac{K_p s + K_i}{s} \tag{8}$$

Here, K_p and K_i are the parameters of the PI controller. The integral term introduces a pole at the origin, ensuring zero steady-state error for a step input. However, it also contributes negative phase, thereby reducing the overall phase margin of the compensated system. As a result, the system exhibits significant oscillations in the output voltage response, which is undesirable. Therefore, the PI controller alone is not an optimal solution for controlling DC-DC converters with poor phase margins [7], [11].

- **Lead compensator**: The transfer function of lead compensator is given as

$$G_{lead}(s) = \frac{K_{lead}(s+\alpha)}{(s+\beta)}, \beta > \alpha \tag{9}$$

Here, K_{lead}, α and β are the parameters of the lead compensator. The lead compensator is primarily used to enhance the system's response speed and bandwidth by introducing positive phase at the desired gain crossover frequency, thereby improving phase margin and transient performance. However, while it effectively enhances stability and accelerates response, its impact on steady-state error correction is limited. This limitation makes it less suitable for applications where minimizing steady-state error is critical, such as DC-DC converters [12].

- **PI-lead controller**: The PI-lead controller combines the effects of PI and lead compensators. Hence, the transfer function of the PI-lead controller is denoted as

$$G_{PI-Lead}(s) = \frac{K_p s + K_i}{s} \cdot \frac{K_{Lead}(s+\alpha)}{(s+\beta)}, \alpha < \beta = \frac{K_i K_{Lead}\left(\frac{s}{K_i/K_p}+1\right)(s+\alpha)}{s(s+\beta)}, \ \alpha < \beta \tag{10}$$

With the new variable $K = K_i K_{Lead}$ and $\omega_z = K_i/K_p$, Equation (10) can be rewritten as

$$G_{PI-Lead}(s) = \frac{K\left(\frac{s}{\omega_z}+1\right)(s+\alpha)}{s(s+\beta)}, \alpha < \beta \tag{11}$$

Here, K, ω_z, α and β are the parameters of PI-lead controller, which are adjusted using the following algorithm.

3.1. Algorithm for PI-Lead Controller Parameters Tuning

In this section, the PI-lead controller is implemented to regulate the output voltage of the non-ideal DC-DC boost converter. A systematic approach is applied to determine the parameters of the PI-lead controller, with simple formulas derived based on the desired phase margin and gain crossover frequency [11].

- **Step 1**: The transfer function of an uncompensated second-order DC-DC converter is given as:

$$G(s) = \frac{b_1 s + b_0}{a_2 s^2 + a_1 s + a_0} \tag{12}$$

This system has constant gain in the low-frequency region and poor phase margin in neighborhood of gain crossover frequency. To improve performance of this system, the PI-lead controller is designed by sharing it in two parts (a) PI controller design and (b) lead compensator design.

- **Step 2**: To improve the gain in low-frequency region, a PI controller $G_{PI}(s)$ is designed. The transfer function of the PI controller is:

$$G_{PI}(s) = \frac{\left(\frac{s}{\omega_z} + 1\right)}{s} \tag{13}$$

Where, ω_z is the corner frequency of the PI controller. In order to improve the low-frequency gain, the corner frequency is selected appropriately lower than the gain crossover frequency. With the PI controller, the compensated second order DC-DC converter is given as:

$$G_1(s) = G(s)G_{PI}(s) = \frac{\left(b_2 + \frac{b_1}{\omega_z}\right)s^2 + \left(b_1 + \frac{b_0}{\omega_z}\right)s + b_0}{a_2 s^3 + a_1 s^2 + a_0 s} \tag{14}$$

The PI compensated system will have zero steady-state error for step input. To improve the transient performance, the lead compensator is designed in the next steps.

- **Step 3**: Specify the desired phase margin φ_{margin} (in degree) and gain crossover frequency ω_{gc} (rad/sec) of overall compensated DC-DC converter system.

Let the magnitude and phase of $G_1(s)$ at gain crossover frequency ω_{gc} are denoted by K_1 and φ_1, respectively i.e.,

$$K_{req} = 1/K_1 \tag{15}$$

$$\varphi_{req} = -180^0 - \varphi_1 + \varphi_{margin} \tag{16}$$

To fulfil the specified phase margin and gain crossover frequency requirements exactly, the lead compensator parameters should be designed to get magnitude K_{req} and phase angle φ_{req} at frequency ω_{gc}.

- **Step 4:** The lead compensator provides the desired phase lead at frequency ω_{gc}. Therefore, the parameters of lead section are designed in such a way that the desired phase boost at ω_{gc} is met exactly. The transfer function of the lead compensator is

$$G_{Lead}(s) = K\frac{s+\alpha}{s+\beta}, \alpha < \beta \tag{17}$$

Magnitude and phase angle of the above transfer function at any frequency 'ω' will be:

$$|G_{Lead}(j\omega)| = K\frac{\sqrt{\omega^2 + \varphi^2}}{\sqrt{\omega^2 + \beta^2}} \tag{18}$$

$$\varphi_{Lead} = \angle G_{Lead}(j\omega) = tan^{-1}\left(\frac{\omega}{\alpha}\right) - tan^{-1}\left(\frac{\omega}{\beta}\right) = tan^{-1}\frac{\omega(\beta-\alpha)}{\omega^2 + \alpha\beta} \tag{19}$$

As $\beta > \alpha$, therefore angle φ_{Lead} is always positive as expected. To find out the frequency (ω_m) at which lead compensator contributes maximum phase angle, differentiating (19) with respect to 'ω', we get.

$$\omega_m = \sqrt{\alpha\beta} \tag{20}$$

By substituting (20) into (18) and (19), magnitude (K_m) and phase angle (φ_m) of lead compensator at frequency $\omega = \omega_m$ are.

$$K_m = K\sqrt{\alpha/\beta} \tag{21}$$

$$\varphi_m = tan^{-1}\frac{\beta-\alpha}{2\sqrt{\alpha\beta}} = sin^{-1}\frac{\beta-\alpha}{\beta+\alpha} \tag{22}$$

This frequency ω_m is chosen as desired gain crossover frequency, ω_{gc}. Therefore, in order to have the desired phase margin at this frequency, the parameters K_m and φ_m must be equal to parameters K_{req} and φ_{req} respectively. Therefore,

$$\omega_{gc}(=\omega_m) = \sqrt{\alpha\beta} \tag{23}$$

$$\varphi_{req}(=\varphi_m) = sin^{-1}\frac{\beta-\alpha}{\beta+\alpha} \tag{24}$$

$$K_{req}(=K_m) = K\sqrt{\alpha/\beta} \tag{25}$$

The PI controller mainly ensures the elimination of steady-state error by increasing the low-frequency gain. However, when applied to non-ideal converters with parasitic elements, the PI controller often restricts the gain crossover frequency, leading to slower dynamic response and prolonged settling time. To overcome these limitations, a lead compensator is designed to provide additional phase margin around the gain crossover frequency, thereby improving system stability and reducing transient duration. Based on this, Equations (23)-(25) are simplified to get the lead compensator parameters (K, α and β) in terms of desired parameters, thus we get.

$$K = K_{req}\sqrt{\frac{1+sin\varphi_{req}}{1-sin\varphi_{req}}} \tag{26}$$

$$\alpha = \omega_{gc}\sqrt{\frac{1-sin\varphi_{req}}{1+sin\varphi_{req}}} \tag{27}$$

$$\beta = \omega_{gc}\sqrt{\frac{1+sin\varphi_{req}}{1-sin\varphi_{req}}} \tag{28}$$

It should be noted that the state-space averaging technique and the general structure of PI-lead tuning (Eqs. (26)-(28)) are adopted from standard control textbooks and previous works such as Shen et al. [11]. The novelty of this study lies in two aspects: (i) the averaged model is extended to explicitly include the parasitic effects of inductors, capacitors, MOSFETs, and diodes, thereby providing a more realistic representation of non-ideal boost converters; and (ii) an algorithm is developed for systematically tuning the PI-lead controller parameters, where the PI term ensures steady-state accuracy and the lead term is adjusted to meet the desired phase margin at the specified gain crossover frequency. This integration provides a practical and effective approach for improving transient response and robustness compared with conventional PI controllers.

3.2. PI-Lead Controller Design for Non-Ideal Boost Converter

The PI-lead structure therefore preserves the PI controller's ability to improve steady-state accuracy, while the lead term enhances the phase margin, resulting in faster transient response and reduced overshoot. Fig. 6 shows the block diagram of PI-lead controlled non-ideal DC-DC boost converter. The performance of the boost converter with PI-lead controller is evaluated for different combinations of ω_z, ω_{gc} and φ_{margin}.

- **Step1**: The duty cycle to output voltage transfer function $G_{vd}(s)$ of the non-ideal DC-DC boost is rewritten as.

$$G_{vd}(s) = \frac{-0.4227s^2 - 1.2812 \times 10^5 s + 9.4057 \times 10^{10}}{s^2 + 4.1760 \times 10^4 s + 3.2433 \times 10^9} \quad (29)$$

The uncompensated loop transfer function $G(s)$ is.

$$G(s) = G_{PWM}(s) * G_{vd}(s) = 1 * G_{vd}(s) = \frac{-0.4227s^2 - 1.2812 \times 10^5 s + 9.4057 \times 10^{10}}{s^2 + 4.1760 \times 10^4 s + 3.2433 \times 10^9} \quad (30)$$

The bode plot of the uncompensated loop transfer function $G(s)$ is shown in Fig. 4. As observed from this figure, the gain crossover frequency is 67 kHz.

- **Step 2**: Design the PI section of PI-lead controller by placing zero (ω_z) at lower frequency sufficiently below than gain crossover frequency of 67 kHz.

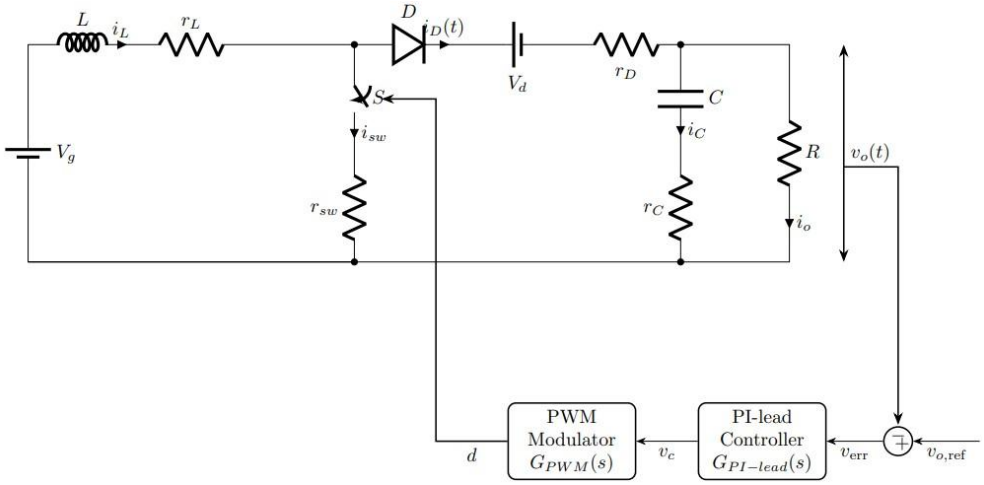

Fig. 6. Detailed schematic of PI-Lead controlled non-ideal DC – DC boost converter

Substituting $\omega_z = 2\pi \times 500$ into (16), the transfer function of PI section is given as.

$$G_{PI}(s) = \frac{(0.0003183s + 1)}{s} \quad (31)$$

The compensated loop transfer function $G_1(s)$ is obtained as.

$$G_1(s) = G_{PI}(s)G_{vd}(s) = \frac{(0.0003183s + 1)}{s} \cdot \frac{-0.4227s^2 - 1.2812 \times 10^5 s + 9.4057 \times 10^{10}}{s^2 + 4.1760 \times 10^4 s + 3.2433 \times 10^9} \quad (32)$$

The frequency response of the transfer function $G_1(s)$ shows that the magnitude K_1 is 0.01 and the phase margin φ_1 is 333.7^0.

- **Step 3:** Define the desired phase margin (φ_{margin}) and gain crossover frequency (ω_{gc} in rad/sec). This design is illustrated for one combination of desired phase margin (φ_{margin}) and gain crossover frequency (ω_{gc} in rad/sec), $\varphi_{margin} = 100^0$ at $\omega_{gc} = 2\pi \times 1500$ rad/sec.
- **Step 4**: Calculate the required gain (K_{req}) and phase boost (φ_{req}).

Substituting K_1, φ_1 and φ_{margin} into (15) and (16) we get $K_{req} = 100$ and $\varphi_{req} = -413^0$.

- **Step 5**: The parameters of lead section are obtained using (26)-(28) as $K = 32.98$, $\alpha = 28765$, and $\beta = 3088$. Therefore, the complete PI-lead controller transfer function is.

$$G_{PI-Lead}(s) = \frac{K\left(\frac{s}{\omega_z} + 1\right)(s + \alpha)}{s(s + \beta)} = \frac{32.98\left(\frac{s}{2\pi \cdot 500} + 1\right)(s + 28765)}{s(s + 3088)} \quad (33)$$

The simulation results not only demonstrate improvements in phase margin and gain crossover frequency but also translate into clear practical advantages. In simple terms, the PI-lead controller provides a faster response, as the output voltage reaches its steady-state level more quickly after a disturbance; it ensures improved stability, by reducing overshoot and avoiding oscillatory behavior; and it enhances robustness, maintaining reliable performance even in the presence of parasitic effects. These characteristics are particularly important for real-world applications such as renewable energy systems and electric vehicles, where both fast transient performance and stable long-term operation are required

The frequency responses of the non-ideal boost converter with PI and PI-lead control design are shown in Fig. 7. This figure shows that the phase margin of the PI lead compensated system is 100° at a gain crossover frequency of 1.5 kHz, while phase margin of the PI compensated system is 100° at a gain crossover frequency of 0.435 kHz, which was the objective of this controller design. The step responses of of PI and PI lead Controlled DC-DC boost converter are shown in Fig. 8. The results show that the PI-lead controller reduces the settling time and overshoot compared to the PI controller, thereby confirming the intended design objectives.

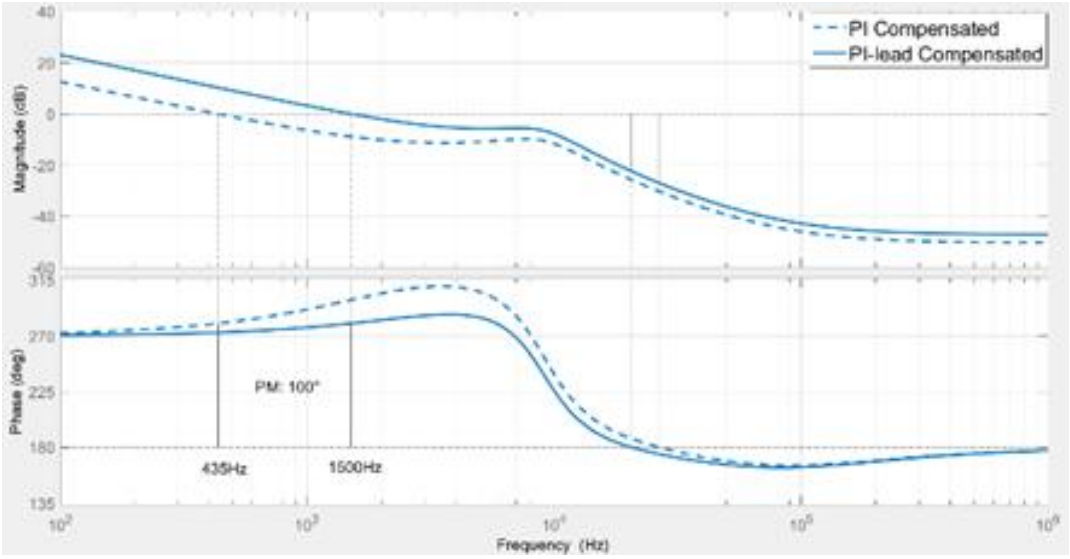

Fig. 7. Comparison of Bode plots of PI and PI lead Controlled DC-DC boost converter with different gain crossover frequency at $\varphi_{margin} = 100^0$

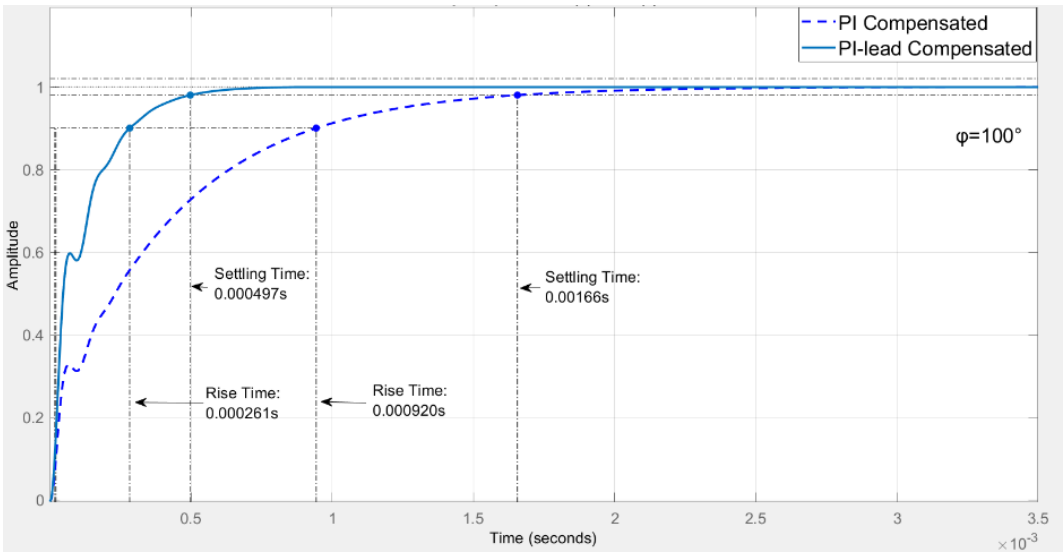

Fig. 8. Comparison of step responses of of PI and PI-lead controlled DC-DC boost converter constant $\varphi_{margin} = 100^0$

In addition to the comparison between PI and PI-lead controllers, it is worth noting that a PID controller, when tuned using standard approaches such as the Ziegler–Nichols method, generally improves the transient response compared to a conventional PI controller but often introduces higher overshoot due to its derivative action. By contrast, the proposed PI-lead controller provides a more balanced trade-off: it enhances transient performance and phase margin without excessive overshoot, while remaining simpler to implement in low-cost embedded systems compared to full PID or more advanced nonlinear controllers. This qualitative assessment is consistent with previous studies on lead-compensated PI structures, and a detailed quantitative comparison is planned for future work.

4. Conclusion

This paper has presented a comprehensive mathematical model of a non-ideal DC-DC boost converter by explicitly incorporating parasitic resistances of inductors, capacitors, MOSFETs, and diodes, as well as the diode forward voltage drop. Using the state-space averaging method, the dynamic equations of the system were derived, providing an accurate foundation for controller design.

To enhance closed-loop performance, a PI-lead controller was developed, with parameters tuned according to desired phase margin and gain crossover frequency. In contrast to the conventional PI controller, the proposed PI-lead compensator ensures both steady-state accuracy and enhanced dynamic behavior in simulation results. Specifically, the PI action minimizes steady-state error, while the lead compensation contributes additional phase margin, thereby helping to reduce overshoot and improve the speed of transient recovery.

The main contributions of this work can be summarized as follows: (1) Development of a non-ideal boost converter model that captures parasitic effects neglected in many previous studies; (2) Introduction of a PI-lead control strategy guided by frequency-domain design criteria; (3) A systematic tuning algorithm for controller parameters based on phase margin and gain crossover frequency; (4) Validation through simulation, demonstrating that the PI-lead controller outperforms conventional PI control in terms of settling response, overshoot reduction, and robustness.

Compared with previous studies, the novelty of this work lies in combining detailed non-ideal modeling with a frequency-domain-based PI-lead design algorithm, providing both theoretical insights and a practical pathway for converter control. The study is currently limited to simulation-based validation at a single operating point. Robustness analysis under parameter variations, load disturbances, and experimental validation remain open tasks for future work. Despite these limitations, the proposed methodology shows promise for applications in renewable energy systems, electric vehicles, and aerospace electronics, where fast and reliable voltage regulation is critical.

Author Contributions: Duc Minh Ngo was primarily responsible for developing the mathematical modeling of the non-ideal DC-DC boost converter and performing the frequency-domain analysis. Dzung Tien Nguyen led the conceptualization of the study, supervised the overall research framework, and provided critical revisions to the manuscript. Thao Thanh Thi Tran contributed to the implementation of simulations, data analysis, and assisted in validating the designed PI-Lead controller. All authors discussed the results, contributed to the interpretation, and approved the final version of the manuscript.

Acknowledgment: This research is supported by Thai Nguyen University of Technology under grant number T2024 - TS19.

Conflicts of Interest: The authors declare no conflict of interest.

References

[1] N. Ghanbari, P. M. Shabestari, A. Mehrizi-Sani and S. Bhattacharya, “State-Space Modeling and Reachability Analysis for a DC Microgrid,” *2019 IEEE Applied Power Electronics Conference and Exposition (APEC)*, pp. 2882-2886, 2019, https://doi.org/10.1109/APEC.2019.8721914.

[2] S. Surya, "Determination of Open Loop Responses of Switched DC–DC Converters Using Various Modeling Techniques," *The Internet of Energy*, pp. 125-153, 2023, https://doi.org/10.1201/9781003399827-7.

[3] W. Zhang, X. Tan, K. Wang, T. Li, and J. Chen, "Design for boost DC-DC converter controller based on state-space average method," *Integrated Ferroelectrics*, vol. 172, no. 1, pp. 152–159, 2016, https://doi.org/10.1080/10584587.2016.1176834.

[4] H. K. Khleaf, A. K. Nahar, and A. S. Jabbar, "Intelligent control of DC-DC converter based on PID-neural network," *International Journal of Power Electronics and Drive Systems*, vol. 10, no. 4, pp. 2254-2262, 2019, http://doi.org/10.11591/ijpeds.v10.i4.pp2254-2262.

[5] M. Z. Hossain, N. A. Rahim, and J. Selvaraj, "Recent progress and development on power DC-DC converter topology, control design and applications: A review," *Renewable and Sustainable Energy Reviews*, vol. 81, pp. 205-230, 2018, https://doi.org/10.1016/j.rser.2017.07.017.

[6] M. U. Khan, A. F. Murtaza, A. M. Noman, H. A. Sher, and M. Zafar, "State-Space Modeling, Design, and Analysis of the DC-DC Converters for PV Application: A Review," *Sustainability*, vol. 16, no. 1, p. 202, 2024, https://doi.org/10.3390/su16010202.

[7] S. Surya and D. B. Singh, "Comparative study of P, PI, PD and PID controllers for operation of a pressure regulating valve in a blow-down wind tunnel," *2019 IEEE International Conference on Distributed Computing, VLSI, Electrical Circuits and Robotics (DISCOVER)*, pp. 1-3, 2019, https://doi.org/10.1109/DISCOVER47552.2019.9007967.

[8] P. Azer and A. Emadi, "Generalized State Space Average Model for Multi-Phase Interleaved Buck, Boost and Buck-Boost DC-DC Converters: Transient, Steady-State and Switching Dynamics," *IEEE Access*, vol. 8, pp. 77735-77745, 2020, https://doi.org/10.1109/ACCESS.2020.2987277.

[9] J. Yao, K. Zheng and A. Abramovitz, "Small-Signal Model of Switched Inductor Boost Converter," *IEEE Transactions on Power Electronics*, vol. 34, no. 5, pp. 4036-4040, 2019, https://doi.org/10.1109/TPEL.2018.2875438.

[10] G. Herbst, "A Building-Block Approach to State-Space Modeling of DC-DC Converter Systems," *J*, vol. 2, no. 3, pp. 247-267, 2019, https://doi.org/10.3390/j2030018.

[11] Y. Shen, Z. Qin, and H. Wang, "Chapter 3 - Modeling and Control of DC-DC Converters," *Control of Power Electronic Converters and Systems*, pp. 69-92, 2018, https://doi.org/10.1016/B978-0-12-805245-7.00003-2.

[12] Y. V. Hote and S. P. Srivastava, "Simple analytical design of lead compensator for Qube servo system," *2017 IEEE 12th International Conference on Power Electronics and Drive Systems (PEDS)*, pp. 53-58, 2017, https://doi.org/10.1109/PEDS.2017.8289148.

[13] A. Amirparast and H. Gholizade-Narm, "Nonlinear robust-optimal control of boost converter in photovoltaic applications," *Advanced Control for Applications: Engineering and Industrial Systems*, vol. 2, no. 4, p. e53, 2020, https://doi.org/10.1002%2Fadc2.53.

[14] S. Agrawal, Atmanandmaya, S. Reddy B. and L. Umanand, "Integration of Photovoltaic Panels with DC Grid Using High Gain DC-DC Converter," *2020 IEEE International Conference on Electronics, Computing and Communication Technologies (CONECCT)*, pp. 1-6, 2020, https://doi.org/10.1109/CONECCT50063.2020.9198618.

[15] A. Reatti, F. Corti, A. Tesi, A. Torlai and M. K. Kazimierczuk, "Effect of Parasitic Components on Dynamic Performance of Power Stages of DC-DC PWM Buck and Boost Converters in CCM," *2019 IEEE International Symposium on Circuits and Systems (ISCAS)*, pp. 1-5, 2019, https://doi.org/10.1109/ISCAS.2019.8702520.

[16] L. Zeng, Y. Chen, B. Zhang and D. Qiu, "Accurate Modeling of the VHF Resonant Boost Converter Considering Multiple Parasitic Parameters," *IEEE Transactions on Power Electronics*, vol. 37, no. 12, pp. 14902-14915, 2022, https://doi.org/10.1109/TPEL.2022.3188576.

[17] M. M. Garg, M. K. Pathak and L. Behera, "Dynamic modeling of a non-ideal DC-DC positive output elementary super-lift Luo converter," *2017 International Conference on Technological Advancements in Power and Energy (TAP Energy)*, pp. 1-6, 2017, https://doi.org/10.1109/TAPENERGY.2017.8397296.

[18] D. Mishra and S. Mandal, "Voltage Regulation of DC-DC Boost Converter using H-infinity Controller," *2020 International Symposium on Devices, Circuits and Systems (ISDCS)*, pp. 1-5, 2020, https://doi.org/10.1109/ISDCS49393.2020.9263019.

[19] A. M. R. Amaral, A. J. M. Cardoso, "Using Python for the Simulation of a Closed-Loop PI Controller for a Buck Converter," *Signals*, vol. 3, no. 2, pp. 313-325, 2022, https://doi.org/10.3390/signals3020020.

[20] K. Panduranga Vittal, S. Bhanja and A. Keshri, "Comparative Study of PI, PID controller for Buck-Boost Converter tuned by Bio-Inspired Optimization Techniques," *2021 IEEE International Conference on Distributed Computing, VLSI, Electrical Circuits and Robotics (DISCOVER)*, pp. 219-224, 2021, https://doi.org/10.1109/DISCOVER52564.2021.9663591.

[21] M. A. Ibrahim, Muhammed, "Performance evaluation of PI controller for positive output Luo converter," *International Journal of Power Electronics and Drive Systems*, vol. 11, no. 4, pp. 1816-1825, 2020, http://doi.org/10.11591/ijpeds.v11.i4.pp1816-1825.

[22] M. E. Albira and M. A. Zohdy, "Adaptive Model Predictive Control for DC-DC Power Converters With Parameters' Uncertainties," *IEEE Access*, vol. 9, pp. 135121-135131, 2021, https://doi.org/10.1109/ACCESS.2021.3113299.

[23] C. Yanarateş, "Optimizing control strategies for DC-DC boost converters: Real-time application of an adaptive gain scheduled ISA-PI controller with hybrid state-space and linear parameter-varying modelling," *PLoS One*, vol. 20, no. 7, p. e0325969, 2025, https://doi.org/10.1371/journal.pone.0325969.

[24] L. Fang, R. Ortega, and R. Griñó, "Voltage Control of the Boost Converter: PI vs. Nonlinear Passivity-Based Control," *International Journal of Robust and Nonlinear Control*, 2025, https://doi.org/10.1002/rnc.70289.

[25] L. Yang, J. Wu, and H. Ma, "Improved adaptive sliding mode control for non-ideal single-inductor dual-output boost converter," *Integration*, vol. 101, p. 102335, 2025, https://doi.org/10.1016/j.vlsi.2024.102335.

[26] A. Choubey, P. K. Padhy and S. K. Jain, "Model Predictive control for DC-DC Boost converter," *2021 IEEE Conference on Energy Conversion (CENCON)*, pp. 58-63, 2021, https://doi.org/10.1109/CENCON51869.2021.9627268.

[27] J. Wu, L. Yang, Z. Lu, and Q. Wang, "Robust adaptive composite control of DC–DC boost converter with constant power load in DC microgrid," *Energy Reports*, vol. 9, pp. 855-865, 2023, https://doi.org/10.1016/j.egyr.2023.04.199.

[28] A. Marmol *et al*., "Dual Control Strategy for Non-Minimum Phase Behavior Mitigation in DC-DC Boost Converters Using Finite Control Set Model Predictive Control and Proportional–Integral Controllers," *Applied Sciences*, vol. 14, no. 22, p. 10318, 2024, https://doi.org/10.3390/app142210318.

[29] F. Mohammadi *et al*., "Robust Control Strategies for Microgrids: A Review," *IEEE Systems Journal*, vol. 16, no. 2, pp. 2401-2412, 2022, https://doi.org/10.1109/JSYST.2021.3077213.

[30] M. Gupta, N. Gupta, M. M. Garg and A. Kumar, "Analysis and Design of PI-Lead Compensator for DC-DC Boost Converter," *2022 4th International Conference on Energy, Power and Environment (ICEPE)*, pp. 1-6, 2022, https://doi.org/10.1109/ICEPE55035.2022.9798141.

[31] S. Prajapati and M. M. Garg, "Fractional-Order PI-Lead Controller Design of DC–DC Power Converter for Renewable Energy Applications," *DC—DC Converters for Future Renewable Energy Systems*, pp. 405-422, 2021, https://doi.org/10.1007/978-981-16-4388-0_22.

[32] S. E. Nwachukwu, "Modelling and Control of a Buck Converter Using State-Space Averaging and Classical Feedback Techniques," *arXiv*, 2025, https://doi.org/10.48550/arXiv.2507.09115.

[33] L. Mitra and U. K. Rout, "Optimal control of a high gain DC-DC converter," *International Journal of Power Electronics and Drive Systems (IJPEDS)*, vol. 13, no. 1, pp. 256-266, 2022, http://doi.org/10.11591/ijpeds.v13.i1.pp256-266.

[34] L. Senapati, A. K. Panda, M. M. Garg and S. K. Mazumder, "Design and Performance Analysis of Cuk SIDO Converter Using PI-Lead Compensator for EV Auxiliary Power Supply," *IEEE Transactions on Industry Applications*, vol. 60, no. 1, pp. 684-693, 2024, https://doi.org/10.1109/TIA.2023.3323423.

[35] M. E. Benzoubir *et al*., "Improved Performance and Voltage Stability of Islanded Inverters Using Single-Loop PI-Lead Controller," *IEEE Access*, vol. 13, pp. 23851-23865, 2025, https://doi.org/10.1109/ACCESS.2025.3537716.

[36] Y. Chen, M. Yang, K. Liu, J. Long, D. Xu and F. Blaabjerg, "Reversed Structure Based PI-Lead Controller Antiwindup Design and Self-Commissioning Strategy for Servo Drive Systems," *IEEE Transactions on Industrial Electronics*, vol. 69, no. 7, pp. 6586-6599, 2022, https://doi.org/10.1109/TIE.2021.3097602.

[37] H. Zeng, Z. Huang, T. Tan, Y. Li and X. Li, "Parasitic-Aware Analysis and Design of a Wideband gm-Boost Low Noise Amplifier at K-Band," *IEEE Transactions on Circuits and Systems II: Express Briefs*, vol. 72, no. 1, pp. 138-142, 2025, https://doi.org/10.1109/TCSII.2024.3485649.

[38] D. Pikulins, S. Tjukovs, and J. Eidaks, "Effects of Control Non-idealities on the Nonlinear Dynamics of Switching DC-DC Converters," *Chaos and Complex Systems*, pp. 117-131, 2020, https://doi.org/10.1007/978-3-030-35441-1_12.

[39] F. Mohan and N. Sasidharan, "A novel state-space model of a non-ideal interleaved boost converter: Impact of operating duty ratio," *Electrical Engineering*, vol. 107, no. 6, pp. 7189-7201, 2025, https://doi.org/10.1007/s00202-024-02932-5.

[40] C. -H. Leong, C. -K. Wong and C. -S. Lam, "An Online ESR Estimation Method for Output Capacitor of DC–DC Boost Converter Without Current Sensor," *IEEE Transactions on Power Electronics*, vol. 40, no. 1, pp. 2196-2209, 2025, https://doi.org/10.1109/TPEL.2024.3470814.

[41] F. J. Vivas, F. Segura, and J. M. Andújar, "Generalized, Complete and Accurate Modeling of Non-Ideal Push–Pull Converters for Power System Analysis and Control," *Applied Sciences*, vol. 13, no. 19, p. 10982, 2023, https://doi.org/10.3390/app131910982.

[42] Z. Zhang *et al*., "High-Efficiency Silicon Carbide-Based Buck-Boost Converter in an Energy Storage System: Minimizing Complexity and Maximizing Efficiency," *IEEE Industry Applications Magazine*, vol. 27, no. 3, pp. 51-62, 2021, https://doi.org/10.1109/MIAS.2020.3024495.

[43] W. Dutta and A. Mallik, "Modeling and Design Optimization of a Bidirectional Ultrahigh Gain DC/DC Converter for Cell-Integrated Power Electronics," *IEEE Journal of Emerging and Selected Topics in Power Electronics*, vol. 13, no. 3, pp. 3297-3310, 2025, https://doi.org/10.1109/JESTPE.2024.3522166.

[44] M. Gupta, N. Gupta, M. M. Garg, and A. Kumar, "Robust control strategies applicable to DC–DC converter with reliability assessment: A review," *Advanced Control for Applications: Engineering and Industrial Systems*, vol. 6, no. 3, p. e217, 2024, https://doi.org/10.1002/adc2.217.

[45] A. El Aroudi, M. Debbat, M. Al-Numay, and A. Abouloiafa, "Fast-Scale Instability and Stabilization by Adaptive Slope Compensation of a PV-Fed Differential Boost Inverter," *Applied Sciences*, vol. 11, no. 5, p. 2106, 2021, https://doi.org/10.3390/app11052106.

[46] V. Repecho, D. Biel, J. M. Olm, and E. Fossas, "Robust sliding mode control of a DC/DC Boost converter with switching frequency regulation," *Journal of the Franklin Institute*, vol. 355, no. 13, pp. 5367–5383, 2018, https://doi.org/10.1016/j.jfranklin.2018.05.028.

[47] O. Ibrahim, N. Z. Yahaya and N. Saad, "Comparative studies of PID controller tuning methods on a DC-DC boost converter," *2016 6th International Conference on Intelligent and Advanced Systems (ICIAS)*, pp. 1-5, 2016, https://doi.org/10.1109/ICIAS.2016.7824044.

[48] P. Verma, M. N. Anwar and G. L. Raja, "Unified Control Strategy for Step-Up DC–DC Converters With User-Defined Robustness," *IEEE Journal of Emerging and Selected Topics in Power Electronics*, vol. 13, no. 5, pp. 5856-5866, 2025, https://doi.org/10.1109/JESTPE.2025.3569772.

[49] K. Doğan and B. Dağ, "Design and Optimization of Voltage Mode PWM Control of DC-DC Buck Converter with a PI-Lead Compensator Using the Simulated Annealing Algorithm," *Black Sea Journal of Engineering and Science*, vol. 7, no. 1, pp. 72-88, 2024, https://doi.org/10.34248/bsengineering.1382392.

[50] K. Najdek and R. Nalepa, "The Frequency- and the Time-Domain Design of a Dual Active Bridge Converter Output Voltage Regulator Based on the D-Decomposition Technique," *IEEE Access*, vol. 9, pp. 71388-71405, 2021, https://doi.org/10.1109/ACCESS.2021.3078410.

[51] A. K. Bonela, M. K. Sarkar, and K. Kumar, "Robust non-fragile control of DC–DC buck converter," *Electrical Engineering*, vol. 106, no. 1, pp. 983-991, 2024, https://doi.org/10.1007/s00202-023-02017-9.

[52] O. Gam, R. Abdelati, M. A. Tankari, M. F. Mimouni and G. Lefebvre, "Comparison of integer and fractional order controller of battery discharge based DC-DC converter," *2016 17th International Conference on Sciences and Techniques of Automatic Control and Computer Engineering (STA)*, pp. 288-297, 2016, https://doi.org/10.1109/STA.2016.7952077.

[53] Y. -S. Hwang, J. -J. Chen, J. -X. Xu, H. -S. Yang, C. -H. Lai and Y. Ku, "An Improved Fast-Transient-Response Low-Transient-Voltage Boost Converter With Pseudo-Current Hysteresis-Controlled Techniques," *IEEE Access*, vol. 9, pp. 127270-127277, 2021, https://doi.org/10.1109/ACCESS.2021.3112065.

[54] O. Shiryayeva, B. Suleimenov, and Y. Kulakova, "Optimal Design of I-PD and PI-D Industrial Controllers Based on Artificial Intelligence Algorithm," *Algorithms*, vol. 17, no. 7, p. 288, 2024, https://doi.org/10.3390/a17070288.

[55] C. González-Castaño, A. Véliz, D. Murillo-Yarce, W. Gil-González, C. Restrepo and A. Garcés, "Passivity-Based Control PI for the Versatile Buck-Boost (VBB) Converter," *IEEE Access*, vol. 12, pp. 110394-110405, 2024, https://doi.org/10.1109/ACCESS.2024.3439688.

[56] M. M. Cane and G. C. Xin, "Design and Analysis of PI Controller for Isolated Bidirectional DC-DC Converter," *2022 IEEE 6th Information Technology and Mechatronics Engineering Conference (ITOEC)*, pp. 1742-1745, 2022, https://doi.org/10.1109/ITOEC53115.2022.9734398.

[57] S. Tavakoli, J. Sadeghi, I. Griffin, and P. J. Fleming, "PI controller tuning for load disturbance rejection using constrained optimization," *International Journal of Dynamics and Control*, vol. 6, no. 1, pp. 188–199, 2018, https://doi.org/10.1007/s40435-016-0290-6.

[58] H. Alrajhi, Y. Al-Harbi, A. Al-Zahrani, S. A. Raza, A. Daraz, and M. Al-Kaabi, "Comprehensive analysis of PI tuning techniques for VSC applications," *Journal of Umm Al-Qura University for Engineering and Architecture*, vol. 16, pp. 599-616, 2025, https://doi.org/10.1007/s43995-025-00139-8.

[59] Z. U. Haq and A. Ali, "Comparative study of Zeta converter and Boost converter Using PI controller," *2021 7th International Conference on Electrical, Electronics and Information Engineering (ICEEIE)*, pp. 54-59, 2021, https://doi.org/10.1109/ICEEIE52663.2021.9616826.

[60] J. Liu, Z. Liu and H. Su, "Passivity-Based PI Control for Receiver Side of Dynamic Wireless Charging System in Electric Vehicles," *IEEE Transactions on Industrial Electronics*, vol. 69, no. 1, pp. 783-794, 2022, https://doi.org/10.1109/TIE.2021.3050350.

[61] V. Siddhartha, Y. V. Hote, and S. Saxena, "Non-ideal modelling and IMC based PID Controller Design of PWM DC-DC Buck Converter," *IFAC-PapersOnLine*, vol. 51, no. 4, pp. 639-644, 2018, https://doi.org/10.1016/j.ifacol.2018.06.168.